Additive Manufacturing 36 (2020) 101511

Contents lists available at ScienceDirect

Additive Manufacturing

journal homepage: www.elsevier.com/locate/addma

Mechanical characterization and constitutive modeling of visco-hyperelasticity of photocured polymers

Yuhai Xiang[a], Cody Schilling[b], Nitesh Arora[a], A.J. Boydston[b], Stephan Rudykh[a,*]

[a] Department of Mechanical Engineering, University of Wisconsin–Madison, Madison, WI 53706, USA
[b] Department of Chemistry, University of Wisconsin–Madison, Madison, WI 53706, USA

ARTICLE INFO

Keywords:
Photo-polymerization
Visco-hyperelasticity
Polymer chains
3D-printing

ABSTRACT

In this work, we study the nonlinear behavior of soft photocured polymers typically used in 3D-printing. We perform experimental testing of 3D-printed samples cured at various controlled light intensities. The experimental data show the dependency of the material elasticity and rate-sensitivity on the curing light intensity. To elucidate these relations, we develop a physically-based visco-hyperelastic model in the continuum thermodynamics framework. In our model, the macroscopic viscoelastic behavior is bridged to the microscopic molecular chain scale. This approach allows us to express the material constants in terms of polymer chain physical parameters. We consider different physical mechanisms governing hyperelasticity and rate-dependent behaviors. The hyperelastic behavior is dictated by the crosslinked network; whereas, the viscous part originates in the free and dangling chains. Based on our experimental data, we illustrate the ability of the new constitutive model to accurately describe the influence of the light intensity on photocured polymer viscoelasticity.

1. Introduction

3D-printing of soft materials has been employed in numerous areas such as tissue engineering [1,2], drug delivery devices [3,4] and soft robots [5]. The technology expands the design space by allowing the fabrication of complicated geometries, composition, and tailored properties [6,7]. A promising soft material fabrication method – Digital Light Processing (DLP) 3D printing – utilizes photo-polymerization in the layer by layer curing process [8–12]. The produced materials typically exhibit rich material nonlinearity and rate-sensitivity [13–15], and their properties are highly dependent on the printing process parameters. Motivated by providing the understanding of the soft digital material behavior, in this work, we develop a new physically-based visco-hyperelastic model in the continuum thermodynamics framework. Previously, Zarrelli et al. [16] – utilizing the Kohlrausch-Williams-Watts (KWW) equations [17] – developed a constitutive model that describes the dynamic relaxation modulus during curing. The model incorporates the four coupled phenomena: photophysics, photochemistry, chemomechanical coupling, and mechanical deformation. A general thermodynamic framework has been proposed by Long et al. [18]; the model allows simulating different mechanisms-induced photochemical-thermal-mechanical coupling behavior of photo-active polymer undergoing finite deformation. Recently, Zhao et al. [19] investigated the effects of oxygen on the stress relaxation and bending actuation of the light-activated polymers. Most recently, Wu et al. [20] studied the evolution of material properties during the photo-polymerization. They applied a phase evolution model to characterize the coupling between mechanical and chemical reactions during the curing process; the developed "multibranch" viscoelastic model captures the nonlinear viscoelastic behavior of the photocured polymer. Sain et al. [21] proposed a thermal-chemo-mechanically coupled constitutive framework for cured glassy thermoset polymer. Yu et al. [22] presented a theoretical framework to consider the effects of light intensity, light wavelength, and photoinitiator concentration on self-healing behavior. The shape distortion of the structures created by DLP 3D printing technology is investigated by using photo-polymerization reaction kinetics and Euler–Bernoulli beam theory [15].

Photo-polymerized polymers frequently exhibit strong nonlinear viscoelastic behavior under finite deformation [20,23]. To model finite deformation viscoelastic behaviors, the so-called phenomenological and physically-based constitutive models are used. While here, we mostly focus on the physically-based models, interested readers are referred to the works by [24–30], among many others.

Physically-based viscoelastic models can be formulated by consideration of the viscous-related micromechanisms, such as the reptational motion of molecular chains [31–33], re-orientation and stretch relaxation of chain segments [34], as well as the breaking and re-attaching of temporary crosslinks [35]. These models, however, include

* Corresponding author.
E-mail address: rudykh@wisc.edu (S. Rudykh).

https://doi.org/10.1016/j.addma.2020.101511
Received 11 May 2020; Received in revised form 27 July 2020; Accepted 2 August 2020
Available online 29 August 2020

fitting parameters that are not directly related to the underlying physical mechanisms. For the thermodynamically consistent models [29,33,34], appropriate restrictions are imposed on their fitting parameters. On the other hand, physically-based models can be developed by directly characterizing the viscous related microscopic structures so that all material constants can be connected to the microscopic quantities [36–41]. For a more detailed discussion of the topic, the readers are referred to the recent review by Xiang et al. [42]. We note that there is a large number of viscoelastic models incorporating finite-deformation, while only a few models consider the specifics of the viscoelasticity in the photocured polymer [20,21,43,44].

In this paper, we develop a finite-deformation physically-based visco-hyperelastic constitutive model for photocured polymers. Our finite-deformation viscoelastic model incorporates the rate-dependent behaviors by considering the microstructure of the polymer, including the crosslinked network, and free and dangling chains (schematically shown in Fig. 3). Moreover, the light intensity-dependent crosslinked network and the nonlinear viscosity of free and dangling chains are also included in the model.

We further apply our model for a particular material – 2-hydroxyethyl acrylate (HEA) – that we produce through DLP 3D-printing with the light intensity-controlled viscoelasticity. We illustrate the ability of the constitutive model to accurately describe the experimentally observed influence of the light intensity on the photocured polymer viscoelasticity.

The paper is organized as follows: Section 2 describes the procedures for 3D printing and mechanical characterization. Section 3 presents the continuum thermodynamic framework for viscoelastic materials, the formulation for light intensity-dependent nonlinear viscosity of the free and dangling chains, and the expressions for light intensity-dependent Helmholtz free energy density. Section 4 includes the modeling and experimental results, followed by discussions and concluding remarks.

2. Material fabrication and experiments

The sample fabrication procedure is schematically shown in Fig. 1. The typical DLP printing system comprises a light projector, moving stage, and a resin vat [8,11,45]. The geometrical features of the specimens are digitally sliced into a series of images. Then, these images

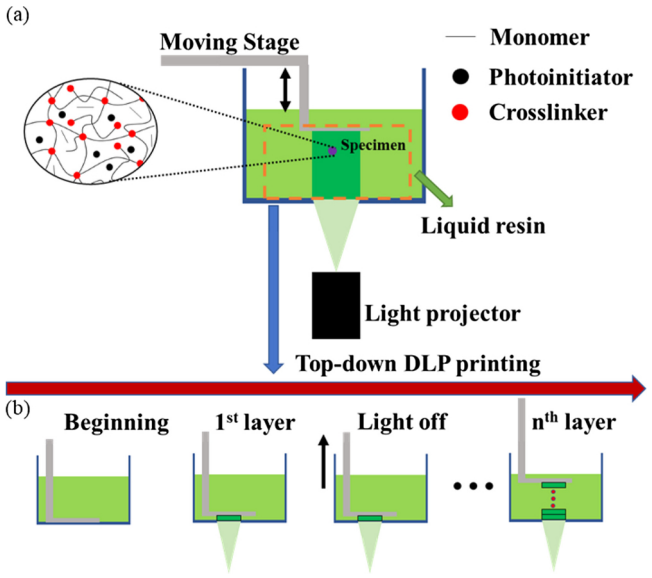

Fig. 1. Schematic representation of the DLP 3D printing process. 3D geometrical images of specimens are sliced into pictures and are projected sequentially into a liquid resin to cure the layer-by-layer structure. (a) The DLP 3D printing system, (b) the procedures for top-down DLP printing.

are sequentially projected by the DLP projector (Optoma HD27 1080p DLP Home projector) into the liquid resin vat to cure it into a solid layer [12]. Thenceforth, the stage moves vertically to a new position, and the next layer is cured. The layer by layer process is repeated until the final structure of the specimen is completely printed (depicted in Fig. 1 (b)).

Specimen preparation. Typical vat photopolymerization resins consist of monomers, crosslinkers, and photoinitiators. Our resin consisted of 2-hydroxyethyl acrylate (HEA) as the monomer and Irgacure 819 as the photoinitiator (0.25 wt % with respect to the monomer mass). No additional crosslinker was added as commercial HEA contains several single weight percent of diacrylate impurities [12]. Different levels of the visible (or white) light intensity I controlled through gray scale adjustments in Microsoft PowerPoint were used to produce specimens with varying mechanical properties, while keeping other environmental variables fixed, including the temperature, the layer exposure time (20 s), the initial concentration of uncured liquid resin and the thickness of each projected layer (100 μm). In particular, we printed the specimens at four different visible (or white) light intensities, namely, I = 12.56 klx± 2.58 klx, 15.10 klx± 4.28 klx, 21.53 klx± 3.37 klx, and 27.17 klx± 3.23 klx. Average intensities were measured using an Extech HD450 Light meter at the vat interface. All printed parts were rinsed with acetone to remove excess monomer and post-cured by irradiating with white light for a minimum of 12 h. For each light intensity, at least 6 dog bone specimens are printed, each comprised of 30 total cured layers. The dimensions of the specimen are provided in Fig. A.1. in Appendix A. To ensure the specimen can be tightly fixed by the screw grippers, two holes at the ends of the specimen (Fig. 2).

Experimental setup. The mechanical testing was performed in the experimental apparatus schematically shown in Fig. 2. The linear actuators and a load cell with Labview are used to synchronize displacement measurement, imaging, and force data collection [46]. The optical system for recording data (consisting of a control computer, camera, a long-distance microscopy lens, polarizing filters, and LED light panels) are installed on a vibration-isolated table, and the collected data is analyzed by the DIC. The DIC camera is aligned to the uniform deformation area in the middle of the specimen. A secondary camera is used to detect possible abnormal deformation conditions. For the uniaxial tensile test, screw-actuated grips are attached to the base of the load frame and the load cell, and the specimen is tightly gripped with the griping-force exerted by the screw grips.

The uniaxial tensile tests were performed at three different strain rates $\dot{\varepsilon} = 10^{-3}s^{-1}$, $10^{-2}s^{-1}$, and $10^{-1}s^{-1}$; the tests were repeated at least twice for each strain rate. The nominal stress P is calculated as $P=F/A_0$, where F is the force data collected by the load cell, and A_0 is the original area of the cross-section of the DIC measured region. The results show that all the HEA specimens tested here exhibit strong viscoelastic behavior.

3. Theory

3.1. The continuum thermodynamics

Consider a polymer molecular network composed of the crosslinked network, free and dangling chains, as schematically shown in Fig. 3. The free chains are not chemically bound to the crosslinked network, while the dangling chains are connected to the crosslinked network by a single end-link. Whereas the crosslinked network is attributed to the purely hyperelastic mechanical response, the free and dangling chains are responsible for the viscous response. The corresponding macroscopic mechanical behavior of the polymer can be described by the rheological model, as shown in Fig. 4. The branches A, B_1 and B_2 represent the crosslinked network, free chains, and dangling chains, respectively.

The deformation acting on all the branches is identical (see, Fig. 4); hence, the applied deformation gradient tensor $\mathbf{F}$ is equal to the deformation gradient tensor of the branch A, B_1 and B_2, i.e.,

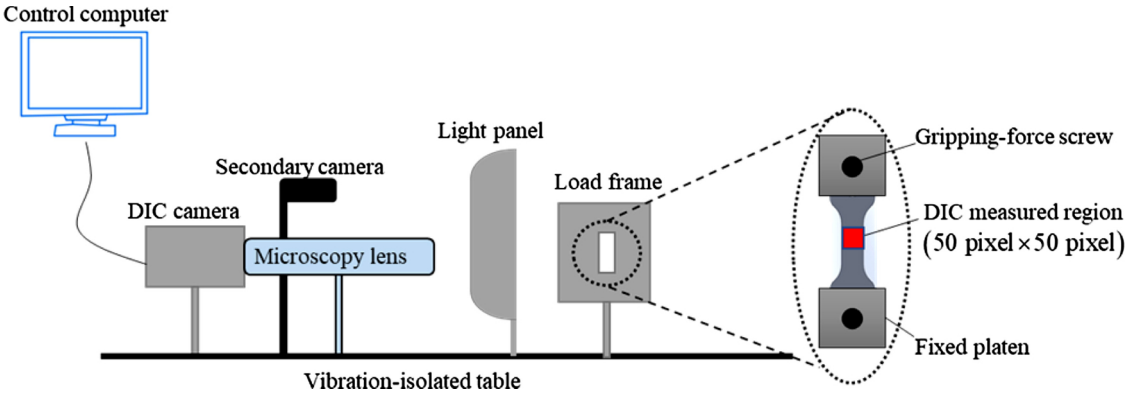

Fig. 2. Schematic of the top and side views of the experimental setup and the front view of the fixtures for the uniaxial tensile test.

$\mathbf{F} = \mathbf{F}_{\mathrm{A}} = \mathbf{F}_{\mathrm{B_1}} = \mathbf{F}_{\mathrm{B_2}}$. For branches $\mathrm{B_1}$ and $\mathrm{B_2}$, the deformation gradient tensor can be multiplicatively decomposed into the elastic part and viscous part as $\mathbf{F}_{\mathrm{B_n}} = \mathbf{F}^{\mathrm{e}}_{\mathrm{B_n}}\mathbf{F}^{\mathrm{i}}_{\mathrm{B_n}}$ (n = 1,2). $\mathbf{F}^{\mathrm{e}}_{\mathrm{B_n}}$ and $\mathbf{F}^{\mathrm{i}}_{\mathrm{B_n}}$ denote the deformation gradient tensor of the spring and dashpot, respectively.

Next, the continuum thermodynamics is introduced to capture the viscoelastic behavior [24,33,47]. The Helmholtz free energy density functions of the springs are $W_{\mathrm{A}}(\mathbf{F}_{\mathrm{A}})$, $W_{\mathrm{B_1}}(\mathbf{F}^{\mathrm{e}}_{\mathrm{B_1}})$ and $W_{\mathrm{B_2}}(\mathbf{F}^{\mathrm{e}}_{\mathrm{B_2}})$, so that the total Helmholtz free energy density of the printed material is

$$W(\mathbf{F}_{\mathrm{A}}, \mathbf{F}^{\mathrm{e}}_{\mathrm{B_1}}, \mathbf{F}^{\mathrm{e}}_{\mathrm{B_2}}) = W_{\mathrm{A}}(\mathbf{F}_{\mathrm{A}}) + W_{\mathrm{B_1}}(\mathbf{F}^{\mathrm{e}}_{\mathrm{B_1}}) + W_{\mathrm{B_2}}(\mathbf{F}^{\mathrm{e}}_{\mathrm{B_2}}) \tag{1}$$

The total Cauchy stress is given by

$$\mathbf{T} = J^{-1}\frac{\partial W}{\partial \mathbf{F}}\mathbf{F}^{T} = \mathbf{T}_{\mathrm{A}} + \sum_{\mathrm{n}=1}^{2}\mathbf{T}_{\mathrm{B_n}} \tag{2}$$

where $J = \det(\mathbf{F})$,

$$\mathbf{T}_{\mathrm{A}} = J^{-1}\frac{\partial W_{\mathrm{A}}(\mathbf{F}_{\mathrm{A}})}{\partial \mathbf{F}}\mathbf{F}^{\mathrm{T}} \tag{3}$$

and

$$\mathbf{T}_{\mathrm{B_n}} = J^{-1}\frac{\partial W_{\mathrm{B_n}}(\mathbf{F}^{\mathrm{e}}_{\mathrm{B_n}})}{\partial \mathbf{F}}\mathbf{F}^{\mathrm{T}} \tag{4}$$

According to the Clausius-Planck inequality [48]

$$\mathbf{P}:\dot{\mathbf{F}} - \dot{W} \geq 0 \tag{5}$$

where, $\mathbf{P}$ is the total first Piola–Kirchhoff stress, we have

$$\left(\mathbf{P} - \frac{\partial W}{\partial \mathbf{F}}\right):\dot{\mathbf{F}} - \sum_{\mathrm{n}=1}^{2}\frac{\partial W}{\partial(\mathbf{F}_{\mathrm{B_n}}\mathbf{H}^{\mathrm{i}}_{\mathrm{B_n}})}:\frac{\partial(\mathbf{F}_{\mathrm{B_n}}\mathbf{H}^{\mathrm{i}}_{\mathrm{B_n}})}{\partial \mathbf{F}^{\mathrm{i}}_{\mathrm{B_n}}}:\dot{\mathbf{F}}^{\mathrm{i}}_{\mathrm{B_n}} \geq 0 \tag{6}$$

where $\mathbf{H}^{\mathrm{i}}_{\mathrm{B_n}}$ is the inverse of $\mathbf{F}^{\mathrm{i}}_{\mathrm{B_n}}$. According to the Eq. (6), we have

$$\mathbf{P} = \frac{\partial W}{\partial \mathbf{F}} \tag{7}$$

and

$$\sum_{\mathrm{n}=1}^{2}\frac{\partial W}{\partial \mathbf{F}^{\mathrm{e}}_{\mathrm{B_n}}}:(\dot{\mathbf{F}}^{\mathrm{e}}_{\mathrm{B_n}}\mathbf{F}^{\mathrm{i}}_{\mathrm{B_n}}\mathbf{H}^{\mathrm{i}}_{\mathrm{B_n}}) \geq 0 \tag{8}$$

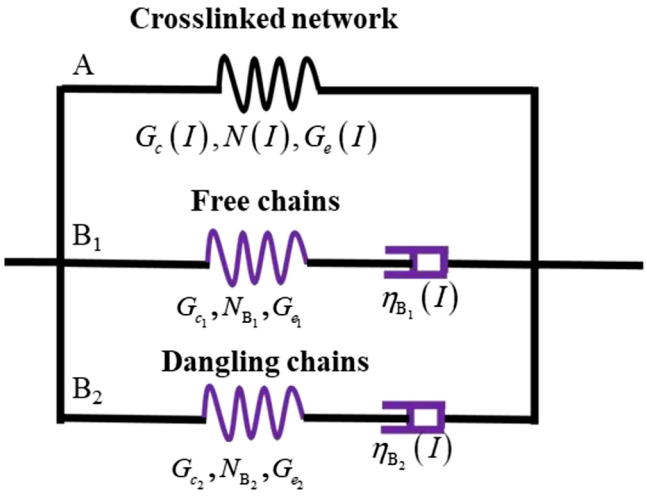

Fig. 4. The macroscopic rheological representation of viscoelasticity.

Introducing the inelastic Cauchy stress

$$\mathbf{T}^{NEQ}_{\mathrm{B_n}} = \frac{1}{\det(\mathbf{F}^{\mathrm{e}}_{\mathrm{B_n}})}\frac{\partial W_{\mathrm{B_n}}(\mathbf{F}^{\mathrm{e}}_{\mathrm{B_n}})}{\partial \mathbf{F}^{\mathrm{e}}_{\mathrm{B_n}}}(\mathbf{F}^{\mathrm{e}}_{\mathrm{B_n}})^{\mathrm{T}} \tag{9}$$

The Eq. (8) can be rewritten as

$$\mathbf{T}^{NEQ}_{\mathrm{B_n}}:\mathbf{L}^{\mathrm{i}}_{\mathrm{B_n}} \geq 0 \tag{10}$$

where $\mathbf{L}^{\mathrm{i}}_{\mathrm{B_n}} = \mathbf{F}^{\mathrm{e}}_{\mathrm{B_n}}\dot{\mathbf{F}}^{\mathrm{i}}_{\mathrm{B_n}}\mathbf{H}^{\mathrm{i}}_{\mathrm{B_n}}\mathbf{H}^{\mathrm{e}}_{\mathrm{B_n}}$, $\mathbf{H}^{\mathrm{e}}_{\mathrm{B_n}}$ is the inverse of $\mathbf{F}^{\mathrm{e}}_{\mathrm{B_n}}$. Due to the symmetry of $\mathbf{T}^{NEQ}_{\mathrm{B_n}}$, the Eq. (10) is rewritten as

$$\mathbf{T}^{NEQ}_{\mathrm{B_n}}:\mathbf{D}^{\mathrm{i}}_{\mathrm{B_n}} \geq 0 \tag{11}$$

where $\mathbf{D}^{\mathrm{i}}_{\mathrm{B_n}} = (\mathbf{L}^{\mathrm{i}}_{\mathrm{B_n}} + (\mathbf{L}^{\mathrm{i}}_{\mathrm{B_n}})^{\mathrm{T}})/2$. To satisfy the Eq. (11), a kinetic evolution equation is given by Hong [24] as

$$\mathbf{D}^{\mathrm{i}}_{\mathrm{B_n}} = \mathbf{M}:\mathbf{T}^{NEQ}_{\mathrm{B_n}} \tag{12}$$

where $\mathbf{M}$ is a positive-definite fourth-order tensor, defined as [47]

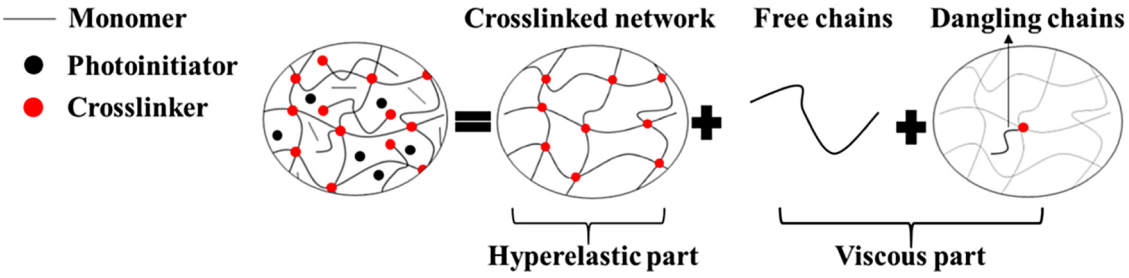

Fig. 3. The schematic diagram of the molecular chain network: the molecular network composed of the crosslinked network, free chains, and dangling chains.

$$\mathbf{M} = \frac{1}{2\eta_{B_n}}\left(\mathbb{I} - \frac{1}{3}\mathbf{I}\otimes\ \mathbf{I}\right) \tag{13}$$

where $\mathbb{I} = \delta_{ik}\delta_{jl}\boldsymbol{e}_i \otimes\ \boldsymbol{e}_j \otimes\ \boldsymbol{e}_k \otimes\ \boldsymbol{e}_l$ is the fourth-order symmetric identity tensor, $\mathbf{I}$ is the second-order identity tensor. η_{B_n} is the viscosity of dashpot B_n (for Eq. (13), the incompressibility of the elastomer is assumed). The procedure for determining the nonlinear viscosity coefficients η_{B_n} is described next; to this end, the viscosity of free chains are determined based on Wu et al. [20] and Zhou et al. [33], and the viscosity of dangling chains is calculated based on Wu et al. [20] and Pearson and Helfand [49].

3.2. The nonlinear viscosity of free chains and dangling chains

3.2.1. Free chains

For describing the free chain contribution, we follow the work of Wu et al. [20]. We assume that the relative viscosity η of melt changes as a function of the degree of conversion of monomers as $\eta = exp(c_p p)$ during curing; here, p is the degree of conversion of monomers, and c_p is a relative viscosity coefficient related to p. Since a higher light intensity can transform more monomers for a given projection time, a higher degree of conversion is produced. Therefore, we assume that the relative viscosity η is the function of light intensity I, namely, $\eta = exp(c_1 I)$, where c_1 is a relative viscosity coefficient related to light intensity. Thus, for the dashpot in the branch B_1 (free chains), the nonlinear viscosity is assumed to be dependent on the light intensity I as

$$\eta_{B_1}(I, \mathbf{F}) = \eta_{B_1}^{I_0}(\mathbf{F})\exp(c_1 I) \tag{14}$$

where c_1 is a relative viscosity coefficient for the dashpot B_1. The relationship between viscosity and deformation is formulated by Zhou et al. [33] as

$$\eta_{B_1}^{I_0}(\mathbf{F}) = \frac{\eta_{B_1}^0}{\alpha(\mathbf{F})^2} \tag{15}$$

where $\eta_{B_1}^0$ is the initial viscosity of the dashpot $\mathbf{B}_1$ in the reference state, and,

$$\alpha(\mathbf{F}) = \frac{\int |\mathbf{F}\cdot\mathbf{R}|^2 f_0(\boldsymbol{R}) d^3\boldsymbol{R}}{\langle \boldsymbol{R}_{ee}^2\rangle_0 \int \frac{|\mathbf{F}\cdot\boldsymbol{u}_0|}{4\pi} d^2\boldsymbol{u}_0} \tag{16}$$

$$\langle \boldsymbol{R}_{ee}^2\rangle_0 = \int |\mathbf{F}\cdot\boldsymbol{R}|^2 f_0(\boldsymbol{R}) d^3\boldsymbol{R} \tag{17}$$

where f_0 is the statistical distribution function of end to end vector $\boldsymbol{R}$ of the free chains (or dangling chains) in the reference state and the Gaussian distribution is usually adopted [33,37]; $\boldsymbol{u}_0$ is the initial unit tangent vector of free chains (or dangling chains).

3.2.2. Dangling chains

Now, we build upon the formulation above Eq. (14), and introduce the contribution of the dangling chains into the material viscoelastic response. For the dashpot in the branch B_2 (dangling chains), similar to the dashpot B_1, the nonlinear viscosity is also formulated as

$$\eta_{B_2}(I, \mathbf{F}) = \eta_{B_2}^{I_0}(\mathbf{F})\exp(c_2 I) \tag{18}$$

where c_2 is a relative viscosity coefficient for the dashpot B_2 and $\eta_{B_2}(\mathbf{F})$ can be expressed by Pearson and Helfand [49] (more details are provided in Appendix B) as

$$\eta_{B_2}^{I_0}(\mathbf{F}) = \eta_{B_2}^0 \alpha(\mathbf{F})\exp\left(\frac{\Gamma'}{\alpha(\mathbf{F})^2}\right) \text{ and } \Gamma' = \frac{12}{25}\Gamma \tag{19}$$

where $\eta_{B_2}^0 = \left(\frac{4\Gamma'}{5}\right)^{-1/2}\frac{b^2 n_{B_2} N_{B_2}\sqrt{\pi}\zeta_{B_2}}{5(\nu')^{5/2}}$ is a parameter related to the viscosity of dashpot B_2, $\nu' = 0.6$ and ζ_{B_2} is the friction constant for dangling chains, $\Gamma = \frac{N_{B_2} b^2}{d_2^2}$ is a tube-related geometrical factor (the arm of dangling chains retract in a confining tube to relax stress), in which b is the length of the Kuhn monomers, and d_2 is the tube diameter of the dangling chains in the reference state.

3.3. Helmholtz free energy density

3.3.1. Crosslinked network

The Helmholtz free energy density W_A of the crosslinked network can be expressed as [50]

$$W_A = G_c(I)N(I)\ln\left(\frac{3N(I) + \frac{1}{2}I_1(\mathbf{C})}{3N(I) - I_1(\mathbf{C})}\right) + G_e(I)\sum_{i=1,2,3}\frac{1}{\lambda_i} \tag{20}$$

where $\mathbf{C} = \mathbf{F}^T\mathbf{F}$ is the right Cauchy-Green tensor of spring A (crosslinked network) and $I_1(\mathbf{C})$ is the first invariant of $\mathbf{C}$; λ_i denotes the principal stretches of spring A. $G_c(I)$ and $G_e(I)$ are the initial elastic moduli corresponding to the responses of the crosslinked network and the entanglement of the spring A, respectively. The moduli are expressed as

$$G_c(I) = n(I)k_B T \text{ and } G_e(I) = \alpha n(I)N(I)k_B T\frac{b^2}{3(d_0(I))^2} \tag{21}$$

where n is the numbers of chains per volume (or chain number density) in the crosslinked network; N is the number of the Kuhn monomers per chain in the crosslinked network; k_B and T are the Boltzmann constant and Kelvin temperature; α is a tube-related geometrical factor; d_0 is the tube diameter of the crosslinked network in the reference state, and it is proportional to $(nNb^2)^{-1}$ [51], so that the entanglement modulus can be expressed as

$$G_e = \frac{\alpha k_B T b^4 (nN)^2}{3\beta} \tag{22}$$

where β is a proportionality factor. The chain density n and number of the Kuhn monomers per chain N of the crosslinked network depends on light intensity. Here, we assume that

$$n = n_0\exp(\alpha_1(I - I_g));\ N = N_0\exp(-\alpha_2(I - I_g));\ (\alpha_1 > 0,\ \alpha_2 > 0) \tag{23}$$

where I_g is the critical light intensity for the gel point[1] ; α_1 and α_2 are light intensity-dependent factors for chain number density and the number of Kuhn monomers per chain of the crosslinked network, respectively; n_0 and N_0 are the number density of chains and the number of the Kuhn monomers per chain in the crosslinked network at the gel point; nN is the number density of monomers of the crosslinked network, and nN increases with an increase in light intensity, thus, $\alpha_1 - \alpha_2 > 0$. Substituting Eq. (23) into (21), we have

$$G_c(I) = G_c^0\exp(\alpha_1(I - I_g)) \text{ and } G_e(I) = G_e^0\exp(2(\alpha_1 - \alpha_2)(I - I_g)) \tag{24}$$

where

$$G_c^0 = n_0 k_B T \text{ and } G_e^0 = \frac{\alpha k_B T b^4 (n_0 N_0)^2}{3\beta} \tag{25}$$

are the initial moduli corresponding to the response of the crosslinked network and the entanglement of the spring A (crosslinked network) at the gel point, respectively. Thus, Eq. (20) can be rewritten as

$$\begin{aligned} W_A = {} & G_c^0\exp(\alpha_1(I - I_g))N_0\exp(-\alpha_2(I \\ & - I_g))\ln\left(\frac{3N_0\exp(-\alpha_2(I - I_g)) + \frac{1}{2}I_1(\mathbf{C})}{3N_0\exp(-\alpha_2(I - I_g)) - I_1(\mathbf{C})}\right) \\ & + G_e^0\exp(2(\alpha_1 - \alpha_2)(I - I_g))\sum_{i=1,2,3}\frac{1}{\lambda_i} \end{aligned} \tag{26}$$

We note that the adopted microstructure-based model for the specific Helmholtz free energy density functions for the crosslinked network W_A [50] will also be used for describing free and dangling chains

[1] The materials are in a liquid state if the light intensities is lower than I_g

W_{B_n}. The model allows us to connect the material parameters to viscous-related microscopic quantities and this characteristic can be further utilized to capture the light intensity-dependent viscoelastic behavior. In addition, the entanglements between chains play an important role in the mechanical behavior of the crosslinked network, free and dangling chains. We note that alternative models, such as 3-chain model [52], Arruda–Boyce model [53], or Gent model [54], could also be used. On the other hand, the utilized model accounts for the entanglement mechanism, thus, potentially improving the accuracy for describing the mechanical behavior of polymer chains.

3.3.2. Free and dangling chains

The hyperelasticity of the free and dangling chains (of the springs in branches B_n (n= 1,2)) is assumed to be governed by a similar Helmholtz free energy density W_{B_n}, namely,

$$W_{B_n} = G_{c_n} N_{B_n} \ln\left(\frac{3N_{B_n} + \frac{1}{2} I_1(\mathbf{C}^e_{B_n})}{3N_{B_n} - I_1(\mathbf{C}^e_{B_n})}\right) + G_{e_n} \sum_{i=1,2,3} \frac{1}{\lambda^e_{i_n}} \tag{27}$$

Here, G_{c_n} and G_{e_n} are initial modulus of the *temporary* crosslinked network and the entanglement modulus of the spring in branches B_n, respectively; N_{B_n} is the number of the Kuhn monomers in a single free or dangling chain; $\mathbf{C}^e_{B_n}$ is the right Cauchy-Green tensor of spring B_n ; $I_1(C^e_{B_n})$ is the first invariant of $C^e_{B_n}$, and $\lambda^e_{i_n}$ represents the principal stretches of spring B_n. Here, we assume the material parameters for spring B_n (temporary hyperelastic properties of free chains and dangling chains) to be independent of light intensity. At certain projection times, high light intensities can transform a more significant number of free chains or dangling chains into the crosslinked network, as compared to low light intensities; however, simultaneously producing more free and dangling chains. Therefore, overall, the light intensities have much more effect on the crosslinked network in comparison to the insignificant effect on the free and dangling chains.

Thus, the combination of Eqs. (2)–(4),(12)–(14),(18),(26), and (27), comprises the visco-hyperelastic constitutive model for photocured polymers.

4. Results

Here, we specify the visco-hyperelastic model for the uniaxial loading and apply the analysis to the experimental data on the 3D-printed HEA polymer material. For the uniaxial tensile deformation, the gradient deformation tensor of the spring A and B_n (shown in Fig. 4) can be expressed as

$$\mathbf{F} = \mathbf{F}_A = \mathbf{F}_{B_n} = \mathbf{F}^e_{B_n}\mathbf{F}^i_{B_n} = \lambda \mathbf{e}_1 \otimes \mathbf{e}_1 + \lambda^{-1/2}(\mathbf{I} - \mathbf{e}_1 \otimes \mathbf{e}_1) \tag{28}$$

$$\mathbf{F}^e_{B_n} = \lambda^e_{B_n} \mathbf{e}_1 \otimes \mathbf{e}_1 + (\lambda^e_{B_n})^{-1/2}(\mathbf{I} - \mathbf{e}_1 \otimes \mathbf{e}_1);\ \mathbf{F}^i_{B_n} = \lambda^i_{B_n} \mathbf{e}_1 \otimes \mathbf{e}_1 + (\lambda^i_{B_n})^{-1/2}(\mathbf{I} - \mathbf{e}_1 \otimes \mathbf{e}_1) \tag{29}$$

where λ represents the uniaxial stretch ratio, the superscripts "*e*" and "*i*" indicate the elastic (spring) and inelastic (viscous dashpot), respectively. Here, we consider the materials to be incompressible.

Substituting Eq. (28) and (29) into Eq.(26) and (27) using Eq. (2), the total nominal stress is determined as

$$\begin{aligned} P_{11}(t) = {} & G^0_c \exp(\alpha_1(I - I_g)) \frac{(\lambda(t) - \lambda^{-2}(t))}{\left(1 - \frac{I_1(t)}{3N_0 \exp(-\alpha_2(I - I_g))}\right)\left(1 + \frac{1}{2}\frac{I_1(t)}{3N_0 \exp(-\alpha_2(I - I_g))}\right)} \\ & + G^0_e \exp(2(\alpha_1 - \alpha_2)(I - I_g))(\lambda^{-1/2}(t) - \lambda^{-2}(t)) \\ & + \sum_{n=1}^{2} G_{c_n} \frac{(\lambda(t)(\lambda^i_{B_n}(t))^{-2} - \lambda^{-2}(t)\lambda^i_{B_n}(t))}{\left(1 - \frac{I_{1e}(t)}{3N_{B_n}}\right)\left(1 + \frac{1}{2}\frac{I_{1e}(t)}{3N_{B_n}}\right)} \\ & + G_{e_n}(\lambda^{-1/2}(t)(\lambda^i_{B_n}(t))^{-1/2} - \lambda^{-2}(t)\lambda^i_{B_n}(t)) \end{aligned} \tag{30}$$

where $I_1 = \lambda^2 + 2\lambda^{-1}$. The first term of Eq.(30) represents the stress of branch A (crosslinked network) and the second term denotes the stress from branches B_1 and B_2 (free chains and dangling chains). Then, substituting the expressions of the viscosity of free chains (14) and dangling chains (18) into the kinetic evolution Eq. (12), we have

$$\begin{aligned} \frac{d\lambda^i_{B_1}(t)}{dt} = {} & \frac{\lambda^i_{B_1}(t)\alpha(\mathbf{F})^2}{3\eta^0_{B_1}\exp(c_1 I)} \left[G_{c_1} \frac{(\lambda^2(t)(\lambda^i_{B_1}(t))^{-2} - \lambda^{-1}(t)\lambda^i_{B_1}(t))}{\left(1 - \frac{I^{B_1}_{1e}(t)}{3N_{B_1}}\right)\left(1 + \frac{1}{2}\frac{I^{B_1}_{1e}(t)}{3N_{B_1}}\right)} \right. \\ & \left. + G_{e_1}(\lambda^{1/2}(t)(\lambda^i_{B_1}(t))^{-1/2} - \lambda^{-1}(t)\lambda^i_{B_1}(t)) \right] \end{aligned} \tag{31}$$

$$\begin{aligned} \frac{d\lambda^i_{B_2}(t)}{dt} = {} & \frac{\lambda^i_{B_2}(t)}{3\eta^0_{B_2}\alpha(F)\exp(\frac{\Gamma}{\alpha(F)^2} + c_2 I)} \left[G_{c_2} \frac{(\lambda^2(t)(\lambda^i_{B_2}(t))^{-2} - \lambda^{-1}(t)\lambda^i_{B_2}(t))}{\left(1 - \frac{I^{B_2}_{1e}(t)}{3N_{B_2}}\right)\left(1 + \frac{1}{2}\frac{I^{B_2}_{1e}(t)}{3N_{B_2}}\right)} \right. \\ & \left. + G_{e_2}(\lambda^{1/2}(t)(\lambda^i_{B_2}(t))^{-1/2} - \lambda^{-1}(t)\lambda^i_{B_2}(t)) \right] \end{aligned} \tag{32}$$

where $I^{B_n}_{1e} = (\lambda^e_{B_n})^2 + 2(\lambda^e_{B_n})^{-1} = \lambda^2(\lambda^i_{B_n})^{-2} + 2\lambda^{-1}\lambda^i_{B_n}$ is the first invariant of the right Cauchy-Green tensor of spring B_n.

The material constants are determined as follows. First, we determine the time-independent material constants G^0_c, α_1, N_0, G^0_e, α and I_g by using the data at a low strain rate ($\dot{\varepsilon} = 10^{-3}s^{-1}$) in Section 4.1. Then, these material constants are used for determining the time-dependent material constants G_{c_1}, N_1, G_{e_1}, $\eta^0_{B_1}$, c_1, G_{c_2}, N_2, G_{e_2}, $\eta^0_{B_2}$, Γ and c_2 by fitting

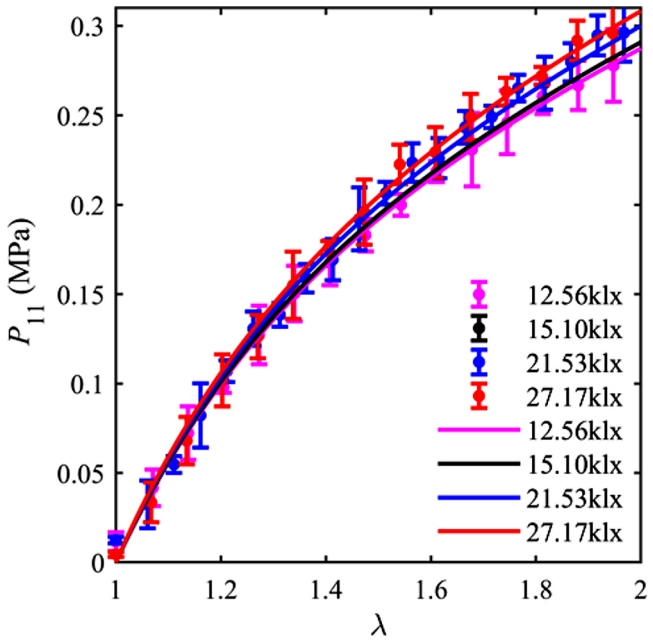

Fig. 5. The model and experimental results for specimens with the strain rate $\dot{\varepsilon} = 10^{-3}s^{-1}$ and different light intensities (12.56 klx, 15.10 klx, 21.53 klx and 27.17 klx). The circles and curves denote the experimental and modeling results, respectively.

Table 1
The material parameters of the hyperelastic (crosslinked network) part of specimens.

G^0_c(MPa)	α_1(1/lx)	N_0	G^0_e(MPa)	α_2(1/lx)	I_g(lx)
0.1048	6.80×10^{-6}	1030	0.1941	6.77×10^{-6}	999

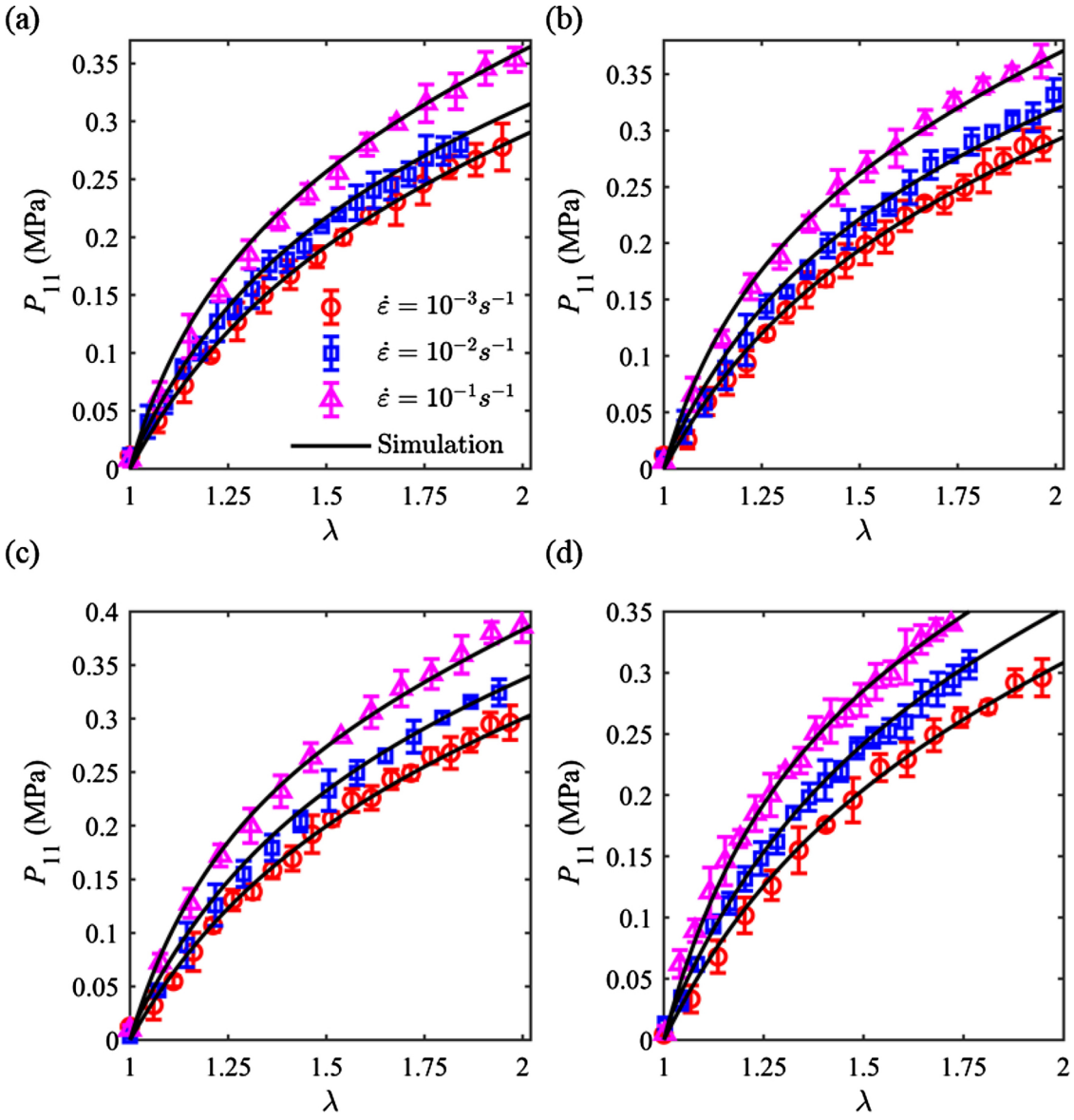

Fig. 6. Comparison of modeling and experimental results for specimens subjected to strain rates $\dot{\varepsilon} = 10^{-3}s^{-1}$ (red circles), $\dot{\varepsilon} = 10^{-2}s^{-1}$ (blue squares), and $\dot{\varepsilon} = 10^{-1}s^{-1}$ (magenta triangles) with projected light intensities (a) $I = 12.56$ klx; (b) $I = 15.10$ klx; (c) $I = 21.53$ klx and (d) $I = 27.17$ klx.

Table 2
The material parameters of the viscoelastic (free and dangling chains) part of specimens.

G_{c_1}(MPa)	N_1	G_{e_1}(MPa)	$\eta^0_{B_1}$(MPa•s)	c_1(1/lx)	G_{c_2}(MPa)	N_2	G_{e_2}(MPa)	$\eta^0_{B_2}$(MPa•s)	Γ'	c_2(1/lx)
0.0117	860	0.2785	0.1867	3.32×10^{-5}	0.0424	769	4.14×10^{-5}	1.26	0.0023	6.66×10^{-5}

the data with strain rates $10^{-2}s^{-1}$ and $10^{-1}s^{-1}$ (Section 4.2). We note that a proper initial guess of material constants is essential, and is based on the physical meaning of the material constants, thus, the parameters need to be positive, and, additionally, $\alpha_1 - \alpha_2 > 0$.

4.1. Material constants of the crosslinked network

Here we use the data of quasistatic deformation at a low strain rate ($\dot{\varepsilon} = 10^{-3}s^{-1}$) to extract the material parameters of the hyperelastic part (crosslinked network). To this end, the first term in Eq. (30) is used. In Fig. 5, we show the comparison of experimental data (circular symbols) and simulation results (curves) for the specimens printed at the light intensities: $I = 12.56$ klx (magenta), 15.10 klx (black), 21.53 klx (blue), and 27.17 klx (red). As expected, the response becomes stiffer as the light intensity is increased. This is also captured by the hyperelastic material model based on the crosslinked network. The obtained material parameters are provided in Table 1.

4.2. Material constants of the free and dangling chains

Once the material constants describing material hyperelasticity are obtained, we can evaluate the material parameters corresponding to the viscoelasticity (related to the free and dangling chains). In Fig. 6, we show the dependence of the nominal stress on the stretch ratio obtained from the uniaxial tests (triangular, square, and circles). In particular, the results are shown for the specimens prepared at light intensities

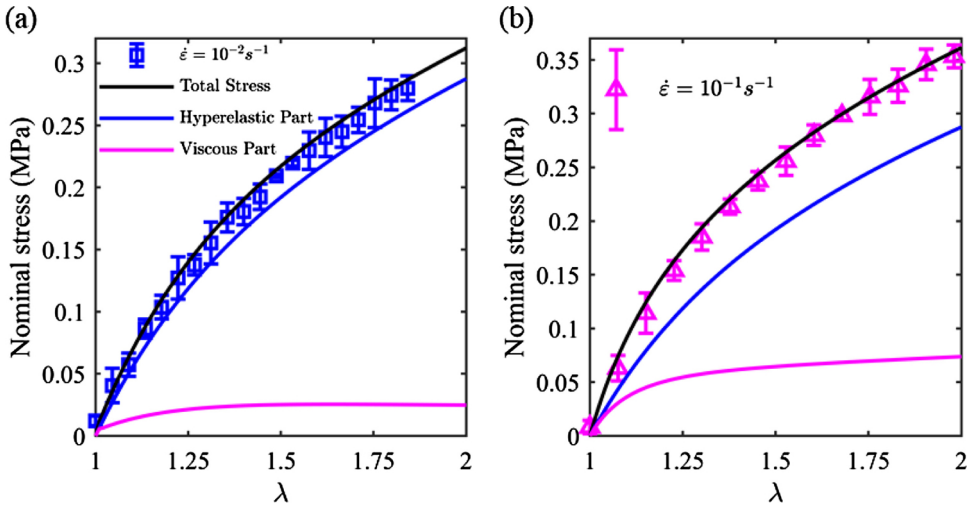

Fig. 7. Comparison of stresses from the hyperelastic part (blue curve) and viscous part (magenta curve) under strain rates (a) $\dot{\varepsilon} = 10^{-2}s^{-1}$ and (b) $\dot{\varepsilon} = 10^{-1}s^{-1}$.

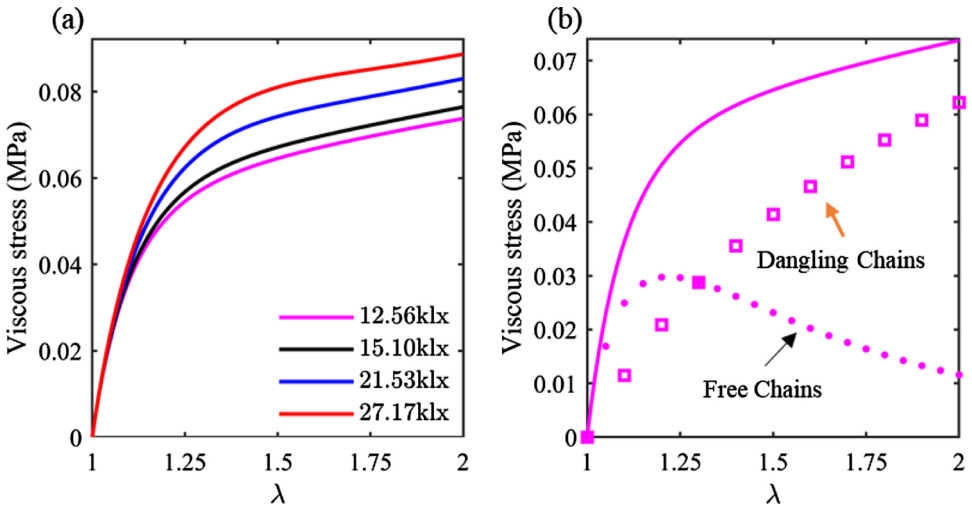

Fig. 8. The viscous stresses of specimens tested at the strain rate $\dot{\varepsilon} = 10^{-1}s^{-1}$. (a) The specimens prepared under light intensities $I = 12.56$ klx, 15.10 klx, 21.53 klx, and 27.17 klx. (b) The viscous stresses from free chains and dangling chains for the specimen with light intensity 12.56 klx.

$I = 12.56$ klx (Fig. 6 (a)), $I = 15.10$ klx (Fig. 6 (b)), $I = 21.53$ klx (Fig. 6 (c)), and $I = 27.17$ klx (Fig. 6 (d)); subjected to strain rates $\dot{\varepsilon} = 10^{-3}s^{-1}$ (red circles), $\dot{\varepsilon} = 10^{-2}s^{-1}$ (blue squares), and $\dot{\varepsilon} = 10^{-1}s^{-1}$ (magenta triangles). We use Eqs. (30)–(32) to simultaneously fit the experimental data for these specimens with strain rates ($10^{-2}s^{-1}$ and $10^{-1}s^{-1}$). The modeling results for the nominal stress-stretch curves are shown in Fig. 6. For completeness, the simulation results for strain rate $\dot{\varepsilon} = 10^{-3}s^{-1}$ are also presented. Clearly, the proposed model can accurately capture light intensity-dependent viscoelastic response. We note that this model feature comes at the cost of introducing additional material parameters, as compared to existing models; for example, Bergström and Boyce [55] model describes the material behavior with only 7 material parameters. On the other hand, our model enables us to capture the light intensity-dependent behavior (although, at the cost of introducing additional material parameters), which is a desirable feature for modeling DLP 3D-printed materials. The corresponding material parameters (for free and dangling chains) are provided in Table 2.

Utilizing the parameters listed in Table 1 and Table 2, we can compare the stress contributions from the crosslinked network, free and dangling chains, and analyze the dependency of nonlinear viscosity on the deformation and light intensity.

To analyze the stress contributions from the crosslinked network, free and dangling chains, we consider the example of the specimens prepared under light intensity $I = 12.56$ klx subjected to strain rates $\dot{\varepsilon} = 10^{-2}s^{-1}$ and $10^{-1}s^{-1}$ (the fitting parameters are listed in Table 1 and Table 2). In Fig. 7, we show the contribution from the hyperelastic (blue curve) and viscous (magenta curve) part to the total stress (black curve). On comparing Fig. 7 (a) and Fig. 7 (b), one can observe that the stress from the viscous part increases with the increase in applied strain rate. Moreover, the contribution from the hyperelastic part is rate-independent for given light intensity.

To elucidate the dependency of viscous response on the light intensity, we consider the example of the specimens tested at the strain rate $\dot{\varepsilon} = 10^{-1}s^{-1}$. Fig. 8 (a) shows the viscous part of the stress for specimens prepared under light intensities $I = 12.56$ klx (magenta), 15.10 klx (black), 21.53 klx (blue), and 27.17 klx (red). Clearly, the viscous stress increases with an increase in light intensity. We also evaluate the contribution from the free chains (magenta circular symbols) and dangling chains (magenta square symbols) to the viscous stresses, separately, as shown in Fig. 8 (b). Here, the specimen prepared under light intensity $I = 12.56$ klx is used as an example. It indicates the importance of both free and dangling chains for accurate characterization of the viscous response. Interestingly, we also observe that the stress of free chains plays a more important role at smaller deformation levels. However, it relaxes much faster than the stress of dangling chains. This observation is in agreement with the fact that the relaxation time of

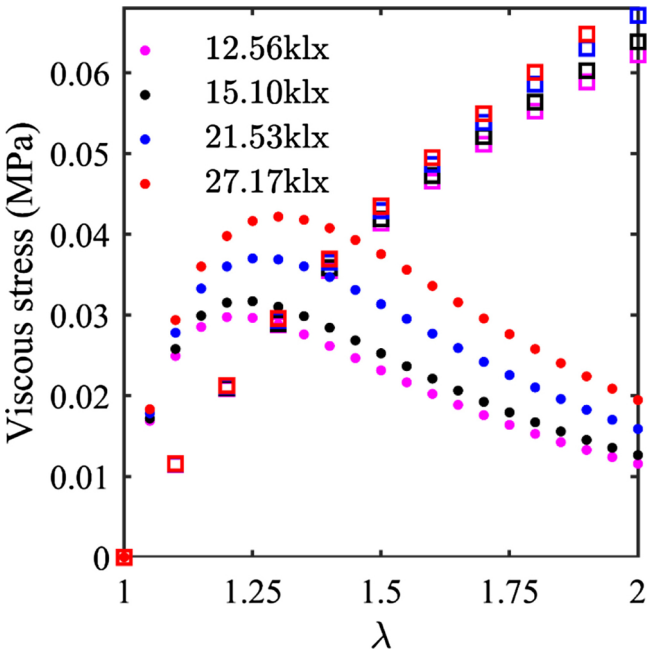

Fig. 9. The stress from free chains and dangling chains; the circular and square symbols respectively represent the results for free chains and dangling chains.

dangling chains is much larger than that of free chains [56,57]. Henceforth, the contribution from dangling chains is more significant than free chains under larger deformations.

Fig. 9 shows the stress from free chains (circular symbols) and dangling chains (square symbols) of the specimens at four light intensities $I = 12.56$ klx (magenta), 15.10 klx (black), 21.53 klx (blue), and 27.17 klx (red). One can observe that the stresses from both the free and dangling chains increase with the increase in light intensity. Moreover, the contribution from free chains shows a higher sensitivity to change in light intensity than dangling chains.

Next, we study how the viscosity of the free and dangling chains evolve with deformation and light intensity. Using Eqs. (14)–(15), and Eqs. (18)–(19) together with the parameters in Table 1 and Table 2, in Fig. 10, we show the variation of nonlinear viscosity of these chains with deformation. We consider four different light intensities: $I = 12.56$ klx (magenta), 15.10 klx (black), 21.53 klx (blue), and 27.17 klx (red). We observe that both the deformation and light intensity significantly affect the viscosity. In particular, the light intensity has a similar effect on the viscosity of both free and dangling chains. More specifically, the viscosity of these chains increases with the increase in light intensity. In contrast, the influence of deformation on the viscosity of free and dangling chains is opposite, i.e., the viscosity of free chain decreases, while that of the dangling chain increases with the increase in deformation.

We show the effect of the number of free chains on the mechanical response of the specimen in Fig. 11. We consider an example of the specimen prepared under light intensity $I = 27.17$ klx tested at the strain rate $\dot{\varepsilon} = 10^{-1}s^{-1}$. To illustrate the model predictions for the polymer behavior with an increased amount of free-chains, we show the results for (i) specimens with unchanged free chains (back curve), and (ii) with the doubled amount of free chains (red curve). We observe that free chains play a more significant role at smaller deformation levels, while the influence on the stress weakens at larger deformation levels. As expected, the viscoelastic stress contributed by free chains rapidly relax to a similar level as can be seen in Fig. 11 (b). The amounts of free chains can be adjusted by, for example, adding non-crosslinkable analogs into specimens, thus, allowing us to regulate the rate-dependent behavior of the printed specimen.

5. Concluding remarks

In this paper, we experimentally and theoretically investigate the curing light intensity-dependent viscoelastic behavior of HEA prepared by the DLP 3D-printing method. The HEA specimens are printed at different light intensities, otherwise with the same environment setting. The tensile tests are conducted on these specimens at various loading rates. The experimental results reveal the strong dependence of the viscoelasticity of HEA on the light intensity. To shed light on the dependence of the material properties of photocured polymers on curing light intensity, we develop a visco-hyperelastic model. The model is based on the continuum thermodynamics with the decomposition of the polymer microstructure response into hyperelastic and viscous parts. The hyperelastic and viscous parts are attributed to the crosslinked network and the diffusion of free and dangling chains, respectively. The developed model is applied to characterize the rate-dependent behavior of the photocured HEA. The simulation results demonstrate the ability of this model to accurately characterize the light intensity-dependent viscoelastic response. In particular, the stresses from the crosslinked network, free chains, and dangling chains are compared, showing the necessity of simultaneously considering the contributions from free and dangling chains for accurately characterizing viscoelasticity. The evolution of viscosity with the deformation and light intensity are also presented to indicate the strong dependence of viscosity on the

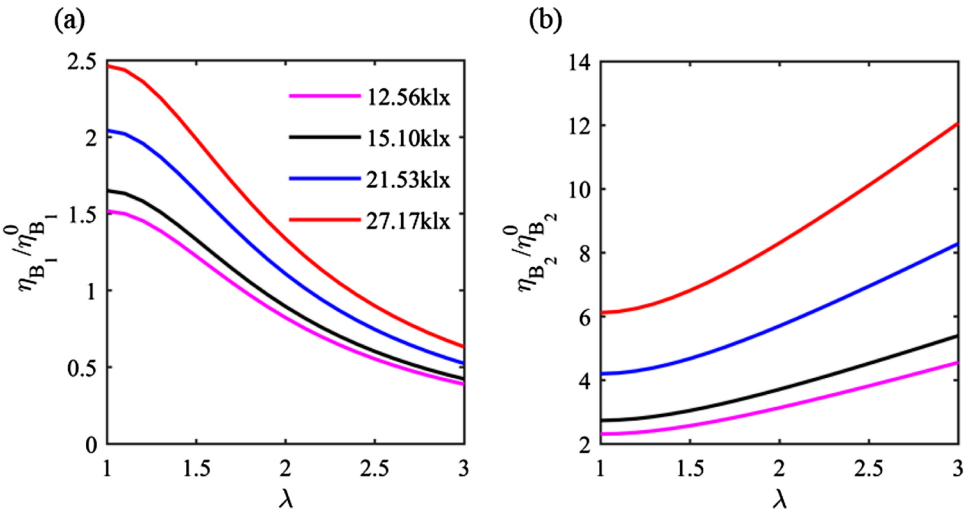

Fig. 10. The dependency of the nonlinear viscosity of (a) free chains and (b) dangling chains on the deformation and light intensities.

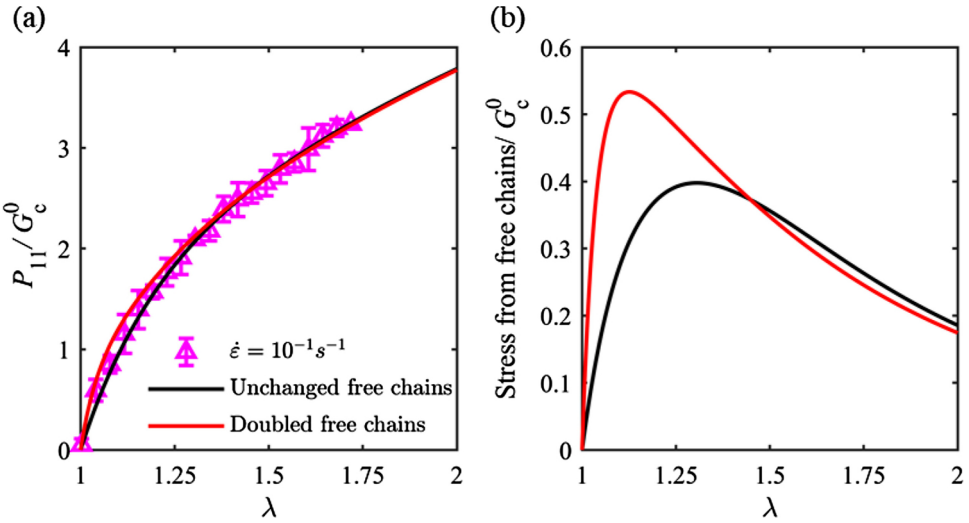

Fig. 11. The stresses of specimens with projected light intensity $I = 27.17$ klx tested at the strain rate $\dot{\varepsilon} = 10^{-1}s^{-1}$. (a) The total stress and (b) the stress from free chains of the free chains unchanged specimen (black curve) and free chains doubled specimen (red curve).

deformation and light intensity. The effect of the free chains on mechanical response is also discussed. Our model predicts that the free chains have a more significant effect on the mechanical response at smaller deformation levels, and their influence weakens at large strain levels. This behavior can be potentially realized in experiments by adding non-crosslinkable analogs into the specimen, thus increasing the free chain content. While the model is calibrated based on the experiment data of HEA, it can be used for a large variety of photocured polymers due to the similarity of the photopolymerization mechanism.

While the present study exclusively investigates the effect of projected light-intensity on the mechanical properties of photo-cured polymers, several other controllable factors influence the digital material behavior, for example, oxygen (through reacting with the radicals and making them inactive, or through inhibiting the photopolymerization reaction [19]), the layer thickness [58], exposure time [59], and the post-curing temperature [60]. Moreover, in multi-material 3D-printing [61,62], depending on the characteristic microstructure size, and printing process, the mixing interphase zone can form. These interphases, while being mechanically invisible, may influence pattern formations in soft composites experiencing local buckling [63]. These factors present a rich research avenue towards the understanding of soft 3D-printed material behavior and its relation to the physical mechanism during 3D-printing.

Author statement

Yuhai Xiang and Nitesh Arora contributed to the model development, experimental characterization and producing the results, Cody Schilling fabricated the samples and controlled the material synthesis process related to the modeling, AJ Boydston, and Stephan Rudykh discussed the research, developed the idea, and oversaw the research. All authors participated in the manuscript composition and discussion.

Declaration of Competing Interest

The authors declare that they have no known competing financial interests or personal relationships that could have appeared to influence the work reported in this paper.

Acknowledgements

The research was partially supported by Grainger Institute for Engineering, by the University of Wisconsin - Madison Office of the Vice Chancellor for Research and Graduate Education with funding from the Wisconsin Alumni Research Foundation. AJB and CAS gratefully acknowledge partial financial support from the Yamamoto Family, and National Science Foundation (DMR-1452726).

Appendix A. The dimensions of specimens

The dimensions of the specimens are shown in Fig. A.1.

Appendix B. The viscosity of dangling chains

To obtain the nonlinear viscosity of dangling chains in Section 3.2.2, here, we briefly illustrate the relation between the viscosity of dangling chains and deformation. Different from the free chains, the reptational motion of dangling chains is suppressed by their crosslinked ends. Arm retraction, as the relaxation mechanisms for arm polymers, is also responsible for the stress relaxation of dangling chains [64-68], therefore, the rate-dependent behaviors of the star arms and dangling chains are equivalent [65,66,xxx68](Campise et al., 2015; Curro et al., 1985; Graessley, 1982; Vega et al., 2005). Here we introduce the theory of Pearson and Helfand (1984), the viscosity 0 of the arms of star polymer in this work is expressed as

where is the friction coefficient of the polymer chains, and can be written as

Batra et al. [64], Campise et al. [65], Curro et al. [66], Vega et al. [67], Vega et al. [68] and Yn-hwang [69].

where M is the molecular weight of an arm; is the molecular weight between entanglements; is estimated as 0.6 (Pearson and Helfand, 1984); N is the number of the Kuhn monomers of an arm; d is the tube diameter, wherein the arms are confined; b is the length of the Kuhn monomers; L is the equilibrium contour length of an arm, which can be expressed by Edwards (1986) as

where Ge is the plateau modulus, which can be expressed as (Edwards, 1986; Yn-hwang, 2003)

where is the mass density of arms, R is the molar gas constant, n is the chain number density of arms. Here we assume that the tube diameter of an arm d have a similar evolution relationship with deformation as free chains, thus, d can be expressed as (Zhou et al., 2018)

where is expressed as the Eq. (16) in Section 3.2.1, d is the tube diameter of the arm

under reference configuration. Hence, Eq. (B.1) can be rewritten as where,

The Eq. (B.6) can be directly applied to Section 3.2.2.

References

[1] B. Derby, Printing and prototyping of tissues and scaffolds, Science 338 (2012) 921–926.
[2] B.K. Gu, D.J. Choi, S.J. Park, M.S. Kim, C.M. Kang, C.-H. Kim, 3-dimensional bio-printing for tissue engineering applications, Biomater. Res. 20 (2016) 12.
[3] Z. Muwaffak, A. Goyanes, V. Clark, A.W. Basit, S.T. Hilton, S. Gaisford, Patient-specific 3D scanned and 3D printed antimicrobial polycaprolactone wound dressings, Int. J. Pharm. 527 (2017) 161–170.
[4] K. Vithani, A. Goyanes, V. Jannin, A.W. Basit, S. Gaisford, B.J. Boyd, An overview of 3D printing technologies for Soft materials and potential opportunities for lipid-based drug delivery systems, Pharm. Res. 36 (2018) 4.
[5] Y. Kim, H. Yuk, R. Zhao, S.A. Chester, X. Zhao, Printing ferromagnetic domains for untethered fast-transforming soft materials, Nature 558 (2018) 274–279.
[6] G.I. Peterson, J.J. Schwartz, D. Zhang, B.M. Weiss, M.A. Ganter, D.W. Storti, A.J. Boydston, Production of materials with spatially-controlled cross-link density via vat photopolymerization, ACS Appl. Mater. Interfaces 8 (2016) 29037–29043.
[7] X. Zheng, H. Lee, T.H. Weisgraber, M. Shusteff, J. DeOtte, E.B. Duoss, J.D. Kuntz, M.M. Biener, Q. Ge, J.A. Jackson, Ultralight, ultrastiff mechanical metamaterials, Science 344 (2014) 1373–1377.
[8] G.A. Appuhamillage, N. Chartrain, V. Meenakshisundaram, K.D. Feller, C.B. Williams, T.E. Long, 110th anniversary: vat photopolymerization-based additive manufacturing: current trends and future directions in materials design, Ind. Eng. Chem. Res. 58 (2019) 15109–15118.
[9] A. Bagheri, J. Jin, Photopolymerization in 3D printing, ACS Applied Polymer Materials 1 (2019) 593–611.
[10] S.H. Kim, Y.K. Yeon, J.M. Lee, J.R. Chao, Y.J. Lee, Y.B. Seo, M.T. Sultan, O.J. Lee, J.S. Lee, S.I. Yoon, I.S. Hong, G. Khang, S.J. Lee, J.J. Yoo, C.H. Park, Precisely printable and biocompatible silk fibroin bioink for digital light processing 3D printing, Nat. Commun. 9 (2018) 1620.
[11] X. Kuang, J. Wu, K. Chen, Z. Zhao, Z. Ding, F. Hu, D. Fang, H.J. Qi, Grayscale digital light processing 3D printing for highly functionally graded materials, Sci. Adv. 5 (2019) eaav5790.
[12] J.J. Schwartz, A.J. Boydston, Multimaterial actinic spatial control 3D and 4D printing, Nat. Commun. 10 (2019) 791.
[13] K. Bootsma, M.M. Fitzgerald, B. Free, E. Dimbath, J. Conjerti, G. Reese, D. Konkolewicz, J.A. Berberich, J.L. Sparks, 3D printing of an interpenetrating network hydrogel material with tunable viscoelastic properties, J. Mech. Behav. Biomed. Mater. 70 (2017) 84–94.
[14] V. Slesarenko, S. Rudykh, Towards mechanical characterization of soft digital materials for multimaterial 3D-printing, Int. J. Eng. Sci. 123 (2018) 62–72.
[15] D. Wu, Z. Zhao, Q. Zhang, H.J. Qi, D. Fang, Mechanics of shape distortion of DLP 3D printed structures during UV post-curing, Soft Matter 15 (2019) 6151–6159.
[16] M. Zarrelli, A.A. Skordos, I.K. Partridge, Toward a constitutive model for cure-dependent modulus of a high temperature epoxy during the cure, Eur. Polym. J. 46 (2010) 1705–1712.
[17] M.F. Shlesinger, Williams-Watts dielectric relaxation: a fractal time stochastic process, J. Stat. Phys. 36 (1984) 639–648.
[18] R. Long, H.J. Qi, M.L. Dunn, Thermodynamics and mechanics of photochemcially reacting polymers, J. Mech. Phys. Solids 61 (2013) 2212–2239.
[19] Z. Zhao, X. Mu, N. Sowan, Y. Pei, C.N. Bowman, H. Jerry Qi, D. Fang, Effects of oxygen on light activation in covalent adaptable network polymers, Soft Matter 11 (2015) 6134–6144.
[20] J. Wu, Z. Zhao, C.M. Hamel, X. Mu, X. Kuang, Z. Guo, H.J. Qi, Evolution of material properties during free radical photopolymerization, J. Mech. Phys. Solids 112 (2018) 25–49.
[21] T. Sain, K. Loeffel, S. Chester, A thermo–chemo–mechanically coupled constitutive model for curing of glassy polymers, J. Mech. Phys. Solids 116 (2018) 267–289.
[22] K. Yu, A. Xin, Q. Wang, Mechanics of light-activated self-healing polymer networks, J. Mech. Phys. Solids 124 (2019) 643–662.
[23] D.L. Naik, R. Kiran, On anisotropy, strain rate and size effects in vat photopolymerization based specimens, Addit. Manuf. 23 (2018) 181–196.
[24] W. Hong, Modeling viscoelastic dielectrics, J. Mech. Phys. Solids 59 (2011) 637–650.
[25] H. Khajehsaeid, Application of fractional time derivatives in modeling the finite deformation viscoelastic behavior of carbon-black filled NR and SBR, Polym. Test. 68 (2018) 110–115.
[26] A. Kumar, O. Lopez-Pamies, On the two-potential constitutive modeling of rubber viscoelastic materials, Cr Mecanique 344 (2016) 102–112.
[27] J. Lubliner, A model of rubber viscoelasticity, Mech. Res. Commun. 12 (1985) 93–99.
[28] Y. Mao, S. Lin, X. Zhao, L. Anand, A large deformation viscoelastic model for double-network hydrogels, J. Mech. Phys. Solids 100 (2017) 103–130.
[29] C. Miehe, S. Göktepe, A micro–macro approach to rubber-like materials. Part II: the micro-sphere model of finite rubber viscoelasticity, J. Mech. Phys. Solids 53 (2005) 2231–2258.
[30] A. Wineman, Nonlinear viscoelastic solids—a review, Math. Mech. Solids 14 (2009) 300–366.
[31] J.S. Bergstrom, M.C. Boyce, Constitutive modeling of the large strain time-dependent behavior of elastomers, J. Mech. Phys. Solids 46 (1998) 931–954.
[32] S.F. Edwards, The Theory of Polymer Dynamics, Oxford Univ. Press, 1986.
[33] J. Zhou, L. Jiang, R.E. Khayat, A micro–macro constitutive model for finite-deformation viscoelasticity of elastomers with nonlinear viscosity, J. Mech. Phys. Solids 110 (2018) 137–154.
[34] C. Linder, M. Tkachuk, C. Miehe, A micromechanically motivated diffusion-based transient network model and its incorporation into finite rubber viscoelasticity, J. Mech. Phys. Solids 59 (2011) 2134–2156.
[35] R. Long, K. Mayumi, C. Creton, T. Narita, C.-Y. Hui, Time dependent behavior of a dual cross-link self-healing gel: theory and experiments, Macromolecules 47 (2014) 7243–7250.
[36] Y. Li, S. Tang, B.C. Abberton, M. Kröger, C. Burkhart, B. Jiang, G.J. Papakonstantopoulos, M. Poldneff, W.K. Liu, A predictive multiscale computational framework for viscoelastic properties of linear polymers, Polymer 53 (2012) 5935–5952.
[37] Y. Li, S. Tang, M. Kroger, W.K. Liu, Molecular simulation guided constitutive modeling on finite strain viscoelasticity of elastomers, J. Mech. Phys. Solids 88 (2016) 204–226.
[38] S. Tang, M. Steven Greene, W.K. Liu, Two-scale mechanism-based theory of nonlinear viscoelasticity, J. Mech. Phys. Solids 60 (2012) 199–226.
[39] W.L. Vandoolaeghe, E.M. Terentjev, Constrained Rouse model of rubber viscoelasticity, J. Chem. Phys. 123 (2005) 34902.
[40] W.L. Vandoolaeghe, E.M. Terentjev, A rouse-tube model of dynamic rubber viscoelasticity, J Phys a-Math Theor 40 (2007) 14725–14744.
[41] Y. Xiang, D. Zhong, P. Wang, T. Yin, H. Zhou, H. Yu, C. Baliga, S. Qu, W. Yang, A physically based visco-hyperelastic constitutive model for soft materials, J. Mech. Phys. Solids 128 (2019) 208–218.
[42] Y. Xiang, D. Zhong, S. Rudykh, H. Zhou, S. Qu, W. Yang, A review of physically-based and thermodynamically-based constitutive models for soft materials, Journal of Applied Mechanics, Accepted Manuscript. (2020).
[43] M. Hossain, Z. Liao, An additively manufactured silicone polymer: thermo-viscoelastic experimental study and computational modelling, Addit. Manuf. 35 (2020) 101395.
[44] M. Hossain, R. Navaratne, D. Perić, 3D printed elastomeric polyurethane: Viscoelastic experimental characterisations and constitutive modelling with non-linear viscosity functions, Int. J. Non. Mech. (2020) 103546.
[45] J. Wu, Z. Zhao, X. Kuang, C.M. Hamel, D. Fang, H.J. Qi, Reversible shape change structures by grayscale pattern 4D printing, Multifunctional Materials 1 (2018) 015002.
[46] A.K. Landauer, X. Li, C. Franck, D.L. Henann, Experimental characterization and hyperelastic constitutive modeling of open-cell elastomeric foams, J. Mech. Phys. Solids 133 (2019) 103701.
[47] S. Reese, S. Govindjee, A theory of finite viscoelasticity and numerical aspects, Int. J. Solids Struct. 35 (1998) 3455–3482.
[48] G.A. Holzapfel, Nonlinear solid mechanics: a continuum approach for engineering science, Meccanica 37 (2002) 489–490.
[49] D.S. Pearson, E. Helfand, Viscoelastic properties of star-shaped polymers, Macromolecules 17 (1984) 888–895.
[50] Y. Xiang, D. Zhong, P. Wang, G. Mao, H. Yu, S. Qu, A general constitutive model of soft elastomers, J. Mech. Phys. Solids 117 (2018) 110–122.
[51] L. Fetters, D. Lohse, D. Richter, T. Witten, A. Zirkel, Connection between polymer molecular weight, density, chain dimensions, and melt viscoelastic properties, Macromolecules 27 (1994) 4639–4647.
[52] H.M. James, E. Guth, Theory of the elastic properties of rubber, J. Chem. Phys. 11 (1943) 455–481.
[53] E.M. Arruda, M.C. Boyce, A three-dimensional constitutive model for the large stretch behavior of rubber elastic materials, J. Mech. Phys. Solids 41 (1993) 389–412.
[54] A.N. Gent, A new constitutive relation for rubber, Rubber Chem Technol 69 (1996) 59–61.
[55] J.S. Bergström, M.C. Boyce, Constitutive modeling of the large strain time-dependent behavior of elastomers, J. Mech. Phys. Solids 46 (1998) 931–954.
[56] W.W. Graessley, Entangled linear, branched and network polymer systems - molecular theories, Adv. Polym. Sci. 47 (1982) 67–117.
[57] H. Yamazaki, M. Takeda, Y. Kohno, H. Ando, K. Urayama, T. Takigawa, Dynamic viscoelasticity of poly(butyl acrylate) elastomers containing dangling chains with controlled lengths, Macromolecules 44 (2011) 8829–8834.
[58] J.H. Lee, R.K. Prud'Homme, I.A. Aksay, Cure depth in photopolymerization: experiments and theory, J. Mater. Res. 16 (2001) 3536–3544.
[59] J. Bonada, A. Muguruza, X. Fernández-Francos, X. Ramis, Influence of exposure time on mechanical properties and photocuring conversion ratios for photosensitive materials used in additive manufacturing, Procedia Manuf. 13 (2017) 762–769.
[60] W.D. Cook, M. Johannson, The influence of postcuring on the fracture properties of photo-cured dimethacrylate based dental composite resin, J. Biomed. Mater. Res. 21 (1987) 979–989.
[61] J. Li, T.D. Pallicity, V. Slesarenko, A. Goshkoderia, S. Rudykh, Domain formations and pattern transitions via instabilities in Soft Heterogeneous materials, Adv. Mater. 31 (2019) 1807309.
[62] J. Li, V. Slesarenko, S. Rudykh, Auxetic multiphase soft composite material design through instabilities with application for acoustic metamaterials, Soft Matter 14 (2018) 6171–6180.
[63] N. Arora, A. Batan, J. Li, V. Slesarenko, S. Rudykh, On the influence of inhomogeneous interphase layers on instabilities in hyperelastic composites, Materials 12 (2019) 763.

[64] A. Batra, C. Cohen, L. Archer, Stress relaxation of end-linked polydimethylsiloxane elastomers with long pendent chains, Macromolecules 38 (2005) 7174–7180.
[65] F. Campise, L.E. Roth, R.H. Acosta, M.A. Villar, E.M. Vallés, G.A. Monti, D.A. Vega, Contribution of linear guest and structural pendant chains to relaxational dynamics in model polymer networks probed by time-domain 1H NMR, Macromolecules 49 (2015) 387–394.
[66] J.G. Curro, D.S. Pearson, E. Helfand, Viscoelasticity of randomly crosslinked polymer networks. Relaxation of dangling chains, Macromolecules 18 (1985) 1157–1162.
[67] D.A. Vega, L.R. Gomez, L.E. Royh, J.A. Ressia, M.A. Villar, E.M. Valles, Arm retraction potential of branched polymers in the absence of dynamic dilution, Phys. Rev. Lett. 95 (2005) 166002.
[68] D.A. Vega, M.A. Villar, J.L. Alessandrini, E.M. Valles, Terminal relaxation of model poly(dimethylsiloxane) networks with pendant chains, Macromolecules 34 (2001) 4591–4596.
[69] L. Yn-hwang, Polymer viscoelasticity: basics, molecular theories and experiments, World Scientific, 2003.